

# Scheduling thermostatically controlled loads to provide regulation capacity based on a learning-based optimal power flow model

Ge Chen, *Student Member, IEEE*, Hongcai Zhang, *Member, IEEE*, Hongxun Hui, *Member, IEEE*, Ningyi Dai, *Senior Member, IEEE*, and Yonghua Song, *Fellow, IEEE*

**Abstract**—Thermostatically controlled load (TCL, such as heating, ventilation, and air conditioning system) is a desirable demand-side flexibility source in distribution networks. It can participate in regulation services and mitigate power imbalances from fluctuating distributed renewable generation. To effectively utilize the load flexibility from spatially and temporally distributed TCLs in a distribution network, it is necessary to consider power flow constraints to avoid possible voltage or current violations. Published works usually adopt optimal power flow models (OPF) to describe these constraints. However, these models require accurate topology of the distribution network that is often unobservable in practice. To bypass this challenge, this paper proposes a novel learning-based OPF to optimize TCLs for regulation services. This method trains three regression multi-layer perceptrons (MLPs) based on the distribution network's historical operation data to replicate its power flow constraints. The trained MLPs are further equivalently reformulated into linear constraints with binary variables so that the optimization problem becomes a mixed-integer linear program that can be effectively solved. Numerical experiments based on the IEEE 123-bus system validate that the proposed method can achieve better TCL power scheduling performance with guaranteed feasibility and optimality than other state-of-art models.

**Index Terms**—Optimal power flow, demand-side feasibility, regulation capacity, neural network, security constraint,

## I. INTRODUCTION

To diminish fossil fuel consumption and mitigate global warming, distributed renewable generation has been broadly integrated into distribution networks. In 2020, newly installed renewable generation capacity has reached to 198 GW [1]. However, the growing penetration of distributed renewable generation provokes a vital threat to system stability since its intermittent and stochastic characteristics probably aggravate the imbalance between the demand- and generation-sides [2]. Thus, more flexible resources are required to participate in regulation services [3], [4].

Operation flexibility is traditionally provided by generating units, such as thermal or gas turbine power plants, which

This paper is funded in part by the Science and Technology Development Fund, Macau SAR (File no. SKL-IOTSC-2021-2023, and File no. 0137/2019/A3), and in part by the National Natural Science Foundation of China under Grant 52007200. (*Corresponding author: Hongcai Zhang.*)

G. Chen, H. Zhang, H. Hui, N. Dai and Y. Song are with the State Key Laboratory of Internet of Things for Smart City and Department of Electrical and Computer Engineering, University of Macau, Macao, 999078 China; H. Zhang is also with the Smart City Research Center, Zhuhai UM Science & Technology Research Institute, Zhuhai, 519031 China (email: hcchang@um.edu.mo).

are usually costly and carbon-intensive [5]. With the progress of information and communication technologies, utilizing demand-side flexibility is becoming feasible and economical [6], [7]. The power consumption of thermostatically controlled loads (TCLs), such as heating, ventilation, and air conditioning (HVAC) systems, accounts for a large share in cities' total power consumption. Due to the inherent heating/cooling storage ability of buildings, power scheduling of TCLs can be adjusted temporally with mild impacts on indoor thermal comforts [8], [9]. Many scholars have focused on how to schedule these TCLs to utilize their load flexibility as the regulation capacity for the minimization of the operation cost. References [10], [11] developed virtual battery models to evaluate or utilize the building thermal flexibility. In [12], a stochastic programming method was proposed to investigate the economic benefits of unlocking building flexibility. Reference [13] proposed a three-stage method to maximize the flexibility provided by district heating systems. In [14], the thermal inertia of district heating systems were exploited to provide flexibility to improve the utilization of distributed renewable generation. Reference [15] developed a model-predictive-control-based optimization framework to coordinate HVAC systems with distribution networks. Reference [16] aggregated multiple demand-side flexibility sources (e.g. HVAC loads, battery systems) in a three phase unbalanced network to support regulation services. References [17], [18] proposed optimal control strategies for the operation of TCLs and confirmed that providing frequency regulation and ensuring occupants' thermal comfort can be achieved simultaneously. In [19], an experiment was conducted to verify that HVAC systems in commercial buildings can serve as frequency reserves providers to tracking automatic generation control signals.

Because many TCLs are usually connected to a distribution network, their operations shall satisfy the distribution network's security operation constraints. However, the majority of the aforementioned papers, e.g. references [10]–[13], [17], [18], do not consider power flow constraints so that the obtained strategies may lead to voltage or current violations. To tackle this challenge, some other papers, e.g. references [14]–[16], adopt optimal power flow (OPF) models to consider the security constraints of distribution networks. However, OPF models require accurate topology information of a distribution network that is often unavailable because of unaware topology changes or inaccurate data maintenance [20].

Due to the widespread use of smart meters, obtaining the

historical operation data (i.e. bus power injections, bus voltages and line currents) becomes easier and cheaper. Thus, data-driven methods are paid attention recently for power scheduling in distribution networks. Generally speaking, three types of model-free methods have been proposed in the published papers to utilize the load flexibility from TCLs. The first type is reinforcement learning (RL) based methods. For example, reference [21] employed RL to maximize residential demand flexibility in distribution networks and reference [22] adopted RL for the control of battery energy storage systems to allay overvoltage issues. RL is fully data-driven and can optimize the power dispatch without topology. However, these RL-based methods require significant iterations of “trial-and-errors” for training, which can be quite expensive and can not guarantee optimality and feasibility theoretically. The second type is called “DeepOPF” proposed in [23]. DeepOPF trained a neural network to build the mapping between nodal power injections and the solution of optimal power flow models so that the solving procedure can be accelerated. However, it requires solutions of an optimal power flow model as data labels to train neural networks, so the topology is still indispensable. The last type is the classification-based method proposed in [24], [25]. This method trained a binary-classification multi-layer perceptron (MLP) to judge whether there is constraint violation with the given decision variables (i.e. judge the feasibility of solutions). Then, the MLP was reformulated into mixed-integer constraints to replicate power flow constraints. This method can also schedule TCLs without the topology because only historical operational data is required for the MLP training. Nevertheless, if we use this method to maximize the regulation capacity from TCLs, then the optimal solution may lie on the classification boundaries of the trained MLP. In that case, a desirable solution can be obtained only if these boundaries are well identified, which needs sufficient data samples near the boundaries. Unfortunately, most of the historical data samples are in normal conditions that are usually far away from boundaries in practice. Thus, this method may not be able to derive high-quality feasible solutions.

To overcome the aforementioned challenges, we propose a novel data-driven OPF model for the power scheduling of TCLs. Our major contributions are threefold:

- 1) We propose a novel learning-based OPF model by replicating power flow constraints and power loss calculation with trained regression MLPs. This model only needs historical operational data but does not require the topology. We further apply this model to the power scheduling of spatial-temporally distributed TCLs to provide regulation capacity to demonstrate its effectiveness.
- 2) We propose a new index called “safe distance,” which quantitatively describes the degree of power flow constraint violations, as prediction targets of the regression MLPs to improve the feasibility of the proposed method. Based on the safe distance, the regression MLPs can well identify the feasible/infeasible boundaries of power flow constraints even without samples near the boundaries.
- 3) Considering that the trained MLPs are intractable, we propose a linearization technique to explicitly convert

them into linear constraints with binary variables. Then, the proposed TCL power scheduling problem subject to power flow constraints (replicated by MLPs) is reformulated into a mixed-integer linear program that can be efficiently solved by the Branch-and-Bound algorithm in off-the-shelf solvers with guaranteed optimality.

Numerical experiments based on the IEEE 123-bus test system are conducted to validate the proposed method. The results show that the proposed method can effectively utilize flexibility from TCLs to provide regulation services and promote renewable generation integration. Furthermore, even without rigorously describe power flow models, the proposed strategy can meet the security operation constraints well.

The remaining parts are organized as follows. Section II describes the problem formulation. Section III presents the construction of the proposed learning-based model. Section IV shows simulation results and Section V concludes this paper.

## II. PROBLEM FORMULATION

We consider a distribution network with multiple buildings equipped with flexible TCLs and distributed renewable generators. In this paper, we focus on how to find an optimal power scheduling strategy of TCLs to reduce their energy costs and even make revenue by providing regulation capacity to power systems. Meanwhile, this strategy shall satisfy the operation security constraints of the distribution network and thermal comfort requirements of the buildings. Without loss of generality, we use HVAC systems and PV generation as examples to represent the TCLs and distributed renewable generation in this paper, respectively.

### A. Modeling of distribution network

*1) Energy cost:* We use  $t \in \mathcal{T}$  to index the  $t$ -th time slot ( $\mathcal{T} = \{1, 2, \dots, T\}$ ) and variable  $G_t^{g,-}$  to represent the net power at the root node (substation) of the distribution network during  $t$ , in kW. Then, the energy cost of the distribution network for each time slot  $EC_t$  can be expressed as follows

$$EC_t = \begin{cases} \eta^{\text{buy}} G_t^{g,-} \Delta t, & G_t^{g,-} \geq 0, \\ \eta^{\text{sell}} G_t^{g,-} \Delta t, & G_t^{g,-} < 0, \end{cases} \quad \forall t \in \mathcal{T}, \quad (1)$$

where  $\Delta t$  is the length of one time slot; parameters  $\eta^{\text{buy}}$  and  $\eta^{\text{sell}}$  represent the per-unit prices of electricity purchasing and selling, in \$/MWh; variable  $G_t^{g,-}$  is the baseline net active power at the substation in time slot  $t$ . To directly express the different purchasing and selling prices in one time, two auxiliary variables  $G_t^{\text{buy}}$  and  $G_t^{\text{sell}}$  are introduced to equivalently express  $G_t^{g,-}$ , as follows

$$G_t^{\text{buy}} - G_t^{\text{sell}} = G_t^{g,-}, \quad G_t^{\text{buy}} \geq 0, \quad G_t^{\text{sell}} \geq 0, \quad \forall t \in \mathcal{T}. \quad (2)$$

Then, Eq. (1) can be expressed as

$$EC_t = (\eta^{\text{buy}} G_t^{\text{buy}} - \eta^{\text{sell}} G_t^{\text{sell}}) \Delta t, \quad \forall t \in \mathcal{T}. \quad (3)$$

*2) Regulation revenue:* The distribution network can utilize TCLs’ load flexibility to provide regulation capacity to the power system and make profit. The corresponding revenue (termed as regulation revenue),  $R_t$ , is determined by the

available capacity of the load flexibility provided by the entire distribution network during  $t$ , which can be expressed as [16]:

$$R_t = r_t^{\text{down}} \text{Cap}_t^{\text{down}} + r_t^{\text{up}} \text{Cap}_t^{\text{up}}, \quad \forall t \in \mathcal{T}, \quad (4)$$

where  $r_t^{\text{down}}$  and  $r_t^{\text{up}}$  are the per-unit regulation down and up prices, in \$/MW;  $\text{Cap}_t^{\text{up}}$  and  $\text{Cap}_t^{\text{down}}$  are the flexibility capacities for regulation up and down during  $t$ . These two capacities represent the capabilities to adjust the profile of the net active power at the substation from the baseline value, which quantifies the operational flexibility provided by TCLs and are defined as follows:

$$\text{Cap}_t^{\text{up}} = G_t^{\text{g},-} - G_t^{\text{g},\vee}, \text{Cap}_t^{\text{down}} = G_t^{\text{g},\wedge} - G_t^{\text{g},-}, \quad \forall t \in \mathcal{T}, \quad (5)$$

$$G_t^{\text{g},\wedge} \leq G_t^{\text{g},-} \leq G_t^{\text{g},\vee}, \quad \forall t \in \mathcal{T}, \quad (6)$$

where variables  $G_t^{\text{g},\wedge}$  and  $G_t^{\text{g},\vee}$  denote the upper and lower bounds of the net active power at the substation. Note the down regulation requires the distribution network to increase its loads, so  $G_t^{\text{g},\wedge} - G_t^{\text{g},-}$  represents the capacity for regulation down. Similarly, the capacity for regulation up is expressed as  $G_t^{\text{g},-} - G_t^{\text{g},\vee}$ . This manner for quantifying operational flexibility is also adopted in some other references, e.g., [10], [16].

According to Eqs. (3) and (4), the energy cost depends on the actual net active power  $G_t^{\text{g},-}$  (the baseline), while the regulation revenue is determined by the capacities for regulation up and down, i.e.,  $\text{Cap}_t^{\text{up}}$  and  $\text{Cap}_t^{\text{down}}$  (these two capacities are constrained by  $G_t^{\text{g},\wedge}$  and  $G_t^{\text{g},\vee}$ ). Thus, the three net active powers, i.e.,  $G_t^{\text{g},-}$ ,  $G_t^{\text{g},\wedge}$  and  $G_t^{\text{g},\vee}$ , will be optimized at once in our problem. We adopt subscripts  $\wedge$ ,  $-$  and  $\vee$  to denote variables relevant to the corresponding scenarios (i.e. baseline scenario for  $G_t^{\text{g},-}$ , upper bound scenario for  $G_t^{\text{g},\wedge}$  and lower bound scenario for  $G_t^{\text{g},\vee}$ ), respectively.

3) *Power flow model:* Conventional power flow models are based on topology information. Since this paper focuses on the radial distribution network, the voltage and current magnitudes can be calculated by the DistFlow model [26], as follows<sup>1</sup>:

$$\begin{cases} \sum_{k \in \mathcal{C}_j} P_{jk,t} = p_{j,t} + P_{ij,t} - r_{ij} I_{ij,t}^2, \\ \sum_{k \in \mathcal{C}_j} Q_{jk,t} = q_{j,t} + Q_{ij,t} - x_{ij} I_{ij,t}^2, \\ V_{j,t}^2 = V_{i,t}^2 - 2(r_{ij} P_{ij,t} + x_{ij} Q_{ij,t}) \\ \quad + (r_{ij}^2 + x_{ij}^2) I_{ij,t}^2, \\ I_{ij,t}^2 = \frac{P_{ij,t}^2 + Q_{ij,t}^2}{V_{i,t}^2}, \\ \forall (i, j) \in \mathcal{B}, \forall t \in \mathcal{T}, \end{cases} \quad (7)$$

where  $P_{ij,t}$  and  $Q_{ij,t}$  are the active and reactive power flows on branch  $(i, j)$ , respectively;  $p_{j,t}$  and  $q_{j,t}$  denote the active and reactive power injections on bus  $j$ , respectively;  $V_{i,t}$  and  $I_{ij,t}$  are the magnitudes of the voltage at bus  $i$  and current on branch  $(i, j)$ , respectively;  $r_{ij}$  and  $x_{ij}$  denotes the resistance and reactance of branch  $(i, j)$ , respectively. Symbol  $\mathcal{B}$  represent the index set of branches. Set  $\mathcal{C}_j$  contains the child bus indexes of bus  $j$ . Based on the power balance, the values of net active powers can be calculated by

$$G_t^{\text{g}} + \mathbf{1}^T \mathbf{p}_t = l_t, \quad \forall t \in \mathcal{T}. \quad (8)$$

<sup>1</sup>We omit the subscript  $\{\wedge, -, \vee\}$  in this subsection for convenience.

where  $\mathbf{p}_t$  and  $l_t$  are the active power injections at each bus (except the slack bus) and total power loss in the distribution network, respectively. The active and reactive power injections at all buses (except the slack bus), i.e.,  $\mathbf{p}_t$  and  $\mathbf{q}_t$ , can be represented by the power generated at the bus minus the power consumed, as follows:

$$\mathbf{p}_t = -\mathbf{p}_t^{\text{HV}} - \mathbf{p}_t^{\text{e}} + \mathbf{G}_t^{\text{PV}}, \quad \mathbf{q}_t = -\mathbf{q}_t^{\text{HV}} - \mathbf{q}_t^{\text{e}}, \quad \forall t \in \mathcal{T}, \quad (9)$$

where  $\mathbf{p}_t^{\text{HV}}$  and  $\mathbf{q}_t^{\text{HV}}$  represent the active and reactive power consumption of HVAC systems;  $\mathbf{p}_t^{\text{e}}$  and  $\mathbf{q}_t^{\text{e}}$  denote the active and reactive base loads (i.e. the loads apart from HVACs). The actual PV generation  $\mathbf{G}_t^{\text{PV}}$  is upper bounded by the available PV power  $G_t^{\text{max}}$  (determined by solar radiation)<sup>2</sup>:

$$\mathbf{G}_t^{\text{PV}} \leq \mathbf{G}_t^{\text{max}}, \quad \forall t \in \mathcal{T}. \quad (10)$$

To ensure the distribution network's security operation, the magnitudes of its bus voltages and line currents shall not violate their allowable ranges:

$$\mathbf{V}_{\min} \leq \mathbf{V}_t \leq \mathbf{V}_{\max}, \quad \mathbf{I}_t \leq \mathbf{I}_{\max}, \quad \forall t \in \mathcal{T}, \quad (11)$$

where  $\mathbf{V}_t$  and  $\mathbf{I}_t$  are the vector forms of  $v_{i,t}$  and  $I_{ij,t}$ , respectively. Vectors  $\mathbf{V}_{\min}$ ,  $\mathbf{V}_{\max}$ , and  $\mathbf{I}_{\max}$  determine the feasible regions of bus voltages and line currents.

When the topology is available, we can calculate the net active power  $G_t^{\text{g}}$  and involve the voltage and current limitations based on the power flow model. However, as mentioned in Section I, the topology is often unknown. In this case, the power flow model can not work properly to ensure the operation security of the distribution network.

## B. Modeling of building thermal dynamics

This subsection models buildings' operational flexibility for providing regulation services based on their inherent thermal inertia [10], [16]. To simplify the problem, we aggregate all buildings in the same distribution node as a large pseudo building. Based on the energy conservation, the indoor temperature dynamics of each pseudo building is

$$C_i \frac{d\theta_{i,t}^{\text{in}}}{dt} = \frac{\theta_t^{\text{out}} - \theta_{i,t}^{\text{in}}}{\lambda_i} + h_{i,t}^{\text{h}} - h_{i,t}^{\text{c}}, \quad \forall i \in \mathcal{I}, \forall t \in \mathcal{T}, \quad (12)$$

where  $i$  is the index of distribution nodes or the corresponding pseudo buildings,  $i \in \mathcal{I}$ ; symbols  $\theta_{i,t}^{\text{in}}$  and  $\theta_t^{\text{out}}$  denote the temperatures of indoor and outdoor environments, in °C, respectively. We use  $h_{i,t}^{\text{h}}$  and  $h_{i,t}^{\text{c}}$  to represent heat load contributed by indoor sources (e.g. humans and electric devices) and cooling supply to building  $i$ , in kW, respectively. Parameter  $C_i$  is the heat capacity of building  $i$ . Parameter  $\lambda_i$  is the thermal resistance between the indoor environment of building  $i$  and the ambience. Eq. (12) can be further transformed into a linear form with the forward difference method, as follows:

$$\begin{aligned} \theta_{i,t}^{\text{in},\{\wedge, -, \vee\}} &= \alpha_i \theta_{i,t-1}^{\text{in},-} + \beta_i (h_{i,t-1}^{\text{h}} - h_{i,t-1}^{\text{c},\{\wedge, -, \vee\}}) \\ &\quad + \gamma_i \theta_{t-1}^{\text{out}}, \quad \forall i \in \mathcal{I}, \forall t \in \mathcal{T}, \end{aligned} \quad (13)$$

<sup>2</sup>Note that we assume the PV generation only outputs active power here. The proposed method can be readily extended to consider reactive PV power.

where  $\alpha_i = 1 - \Delta t/(R_i C_i)$ ,  $\beta_i = \Delta t/C_i$  and  $\gamma_i = \Delta t/(R_i C_i)$ . Note that the indoor temperature in the previous time slot is  $\theta_{i,t-1}^{\text{in},-}$  for all the three scenarios rather than  $\theta_{i,t-1}^{\text{in},\{\wedge,-,\vee\}}$  because the regulation up/down capacities are always calculated based on the baseline working state. To prevent thermal discomforts, the indoor temperature should be restricted in a proper range

$$\underline{\theta} \leq \theta_{i,t}^{\text{in},\{\wedge,-,\vee\}} \leq \bar{\theta}, \quad \forall i \in \mathcal{I}, \forall t \in \mathcal{T}, \quad (14)$$

where  $\underline{\theta}$  and  $\bar{\theta}$  are the lower and upper bounds of comfortable range, respectively. The active and reactive power consumption of HVAC systems are in proportion to the cooling supply

$$p_{i,t}^{\text{HV},\{\wedge,-,\vee\}} = h_{i,t}^{\text{c},\{\wedge,-,\vee\}} / COP_i, \quad \forall i \in \mathcal{I}, \forall t \in \mathcal{T}, \quad (15)$$

$$q_{i,t}^{\text{HV},\{\wedge,-,\vee\}} = \phi_i \cdot p_{i,t}^{\text{HV}}, \quad \forall i \in \mathcal{I}, \forall t \in \mathcal{T}, \quad (16)$$

where  $COP_i$  denotes the coefficient of performance of HVAC system; parameter  $\phi_i$  is the ratio of HVAC's active load to the corresponding reactive load. Due to device limitations, the active and reactive power consumption of HVAC systems should be upper bounded by their maximum allowable values:

$$p_t^{\text{HV},\{\wedge,-,\vee\}} \leq \bar{p}, \quad q_t^{\text{HV},\{\wedge,-,\vee\}} \leq \bar{q}, \quad \forall t \in \mathcal{T}. \quad (17)$$

### C. Optimization problem formulation

We aim to schedule the cooling supply to minimize the energy cost minus regulation revenue. Meanwhile, the operational security constraints of the distribution network and the indoor thermal comforts of the buildings should not be violated after applying our TCL power scheduling strategy. Thus, the optimization problem is expressed as

$$\min_{q_t^c, \forall t \in \mathcal{T}} \sum_{t=1}^T (EC_t - R_t), \quad (\mathbf{P1})$$

s.t. Eqs. (2)-(6),  $\{(7)-(11)\}^{\{\wedge,-,\vee\}}$ , (13)-(17).

We use superscript  $\{\wedge,-,\vee\}$  to mark the constraints in triplicate. For example,  $(7)^{\{\wedge,-,\vee\}}$  represents that constraint (20) will be replicated three times for the baseline, upper bound and lower bound scenarios, respectively. Eqs. (2)-(3) describe the calculation method of energy cost; Eqs. (4)-(6) calculate the available regulation capacities; Eqs. (7)-(11) present power flow constraints and Eqs. (13)-(17) represent the building thermal dynamics. By solving **P1**, we can quantify the feasibility of TCLs based on Eq. (5) and obtain the best operational strategy.

Unfortunately, solving **P1** is challenging because it is based on the power flow model and needs accurate topology information of the distribution network that is often unavailable. Without the topology, we can not even establish the power flow constraints successfully. In this case, solving **P1** may become an impossible task. On the contrary, the historical data (i.e. power injections, bus voltages, and line currents) is easy to acquire with low costs due to the widespread use of smart meters. Thus, we propose a data-driven learning-based method to tackle it in the following section.

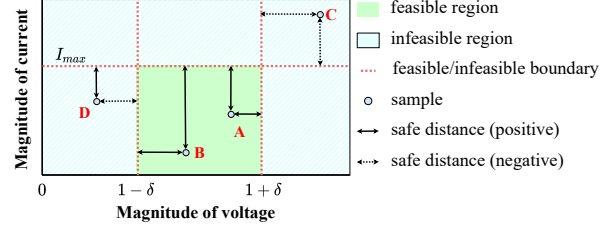


Fig. 1. Schematic diagram of the safe distances. Both of the points A and B locate in the safe region with positive safe distances. Point B has larger safe distances compared to point A. Both of the points C and D lie in the unsafe region with at least one negative safe distance.

## III. LEARNING-BASED OPTIMIZATION MODEL

### A. Safe distance of security constraint

Firstly, in order to qualitatively describe the level of security constraint violations, we introduce two indicators,  $d_t^v$  and  $d_t^c$ , to describe the voltage and current safe margins, termed as “safe distances”, as follows:

$$d_t^v = \delta - \max\{|V_{i,t} - 1|, \forall i \in \mathcal{I}\}, \quad \forall t \in \mathcal{T}, \quad (18)$$

$$d_t^c = \min\{1 - I_{ij,t}/I_{ij,\max}, \forall (i,j) \in \mathcal{B}\}, \quad \forall t \in \mathcal{T}, \quad (19)$$

where, parameter  $\delta$  is the allowable maximum bus voltage fluctuation (e.g. if the allowable voltage range is [0.9 p.u., 1.1 p.u.], then  $\delta = 0.1$  p.u.); parameter  $I_{ij,\max}$  is the maximum allowable magnitude of line current on branch  $(i, j)$ . Note the safe distances in Eqs. (18) and (19) are based on the magnitude values. Thus, even if the current is a complex number or becomes negative, the violations of the line current limitation can still be obtained based on Eq. (19).

Obviously, the security constraint (11) can be satisfied only if all safe distances defined above are nonnegative:

$$d_t^v \geq 0, \quad d_t^c \geq 0, \quad \forall t \in \mathcal{T}. \quad (20)$$

The voltage and current violations can be expressed as

$$\psi_t^v = \max\{-d_t^v, 0\}, \quad \psi_t^c = \max\{-d_t^c, 0\}, \quad \forall t \in \mathcal{T}. \quad (21)$$

Fig. 1 is the schematic of the safe distances, in which the “safe region” refers to the space that has no violated security constraint. The horizontal and vertical axes represent the magnitudes of the line current and bus voltage, respectively.

### B. Learning-based model for replicating security constraints

We assume that the historical data (i.e. power injections, bus voltages and line currents) is available. Instead of using the power flow model to build the voltage and current limitation, i.e. Eq. (11), we train two regression MLPs to predict the voltage and current safe distances, respectively. A typical MLP is composed of one input layer,  $K$  hidden layers, and one output layer, as shown in Fig. 2. Each neuron is made up of one linear mapping and a nonlinear activation function. In this paper, ReLU is employed as our activation function. Symbols  $k$  and  $n_k$  are used to index the hidden layers ( $k \in \mathcal{K} = \{1, \dots, K\}$ ) and neurons in the  $k$ -th hidden layer ( $n_k \in \mathcal{N}_k = \{1, \dots, N_k\}$ ). The inputs of MLPs are defined

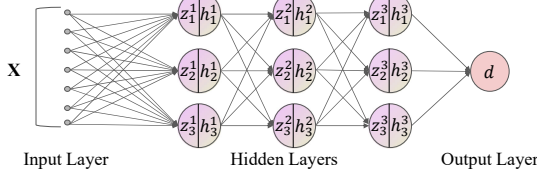


Fig. 2. Structure of an example MLP with 3 hidden layers. Each hidden layer is composed of 3 neurons. Symbols  $z_n^k$  and  $h_n^k$  represent the outputs of the linear mapping and activation function at the  $n$ -th neuron in layer  $k$ , respectively. Symbol  $d$  is the final output of this MLP.

as the active and reactive power injections defined in Eq. (9), which are controllable variables, as follows:

$$\mathbf{x}_t = [\mathbf{p}_t, \mathbf{q}_t], \quad \forall t \in \mathcal{T}. \quad (22)$$

Then, the safe distances  $d_t^{\{v,c\}}$  can be predicated by two different regression MLPs, as follows:

$$\mathbf{h}_t^{0,\{v,c\}} = \mathbf{x}_t, \quad \forall t \in \mathcal{T}, \quad (23)$$

$$\mathbf{z}_t^{k,\{v,c\}} = \mathbf{W}^{k,\{v,c\}} \mathbf{h}_t^{k-1,\{v,c\}} + \mathbf{b}^{k,\{v,c\}}, \quad \forall k \in \mathcal{K}^{\{v,c\}}, \forall t \in \mathcal{T}, \quad (24)$$

$$\mathbf{h}_t^{k,\{v,c\}} = \max(\mathbf{z}_t^{k,\{v,c\}}, 0), \quad \forall k \in \mathcal{K}^{\{v,c\}}, \forall t \in \mathcal{T}, \quad (25)$$

$$d_t^{\{v,c\}} = \mathbf{W}^{K+1,\{v,c\}} \mathbf{h}_t^K + \mathbf{b}^{K+1,\{v,c\}}, \quad \forall t \in \mathcal{T}, \quad (26)$$

where  $\mathbf{h}_t^k \in \mathbb{R}^{N_k}$  is the output of layer  $k$ ; parameters  $\mathbf{W}^k \in \mathbb{R}^{N_k \times N_{k-1}}$  and  $\mathbf{b}^k \in \mathbb{R}^{N_k}$  are the weight matrix and bias of layer  $k$ , which are parameters to be trained. Eq. (23) defines the input layers of the two MLPs; Eqs. (24) and (25) define the linear mapping and nonlinear activation functions in each hidden layer, respectively; Eq. (26) defines the output layer. We add subscript  $\{v,c\}$  in these equations to express two MLPs (one for voltage and one for current) as an unified form. For example, equation  $\mathbf{h}_t^{0,\{v,c\}} = \mathbf{x}_t$  in Eq. (23) is equivalent to  $\mathbf{h}_t^{0,v} = \mathbf{x}_t$  and  $\mathbf{h}_t^{0,c} = \mathbf{x}_t$ .

We present an example case here to demonstrate why the proposed method can achieve better performance than the state-of-art classification-based method. Suppose that the historical samples are distributed as shown in Fig. 3, and the true feasible/infeasible boundary is b. Then, no matter which line in the candidates (i.e. lines a, b, and c) are predicted as the boundary, the classification accuracy is always 100%. However, if line a is chosen as the boundary, then the space between a and b can no longer serve as the feasible region in this method, so the corresponding solution may be overly conservative. If line c is treated as the boundary, then the feasibility of solutions can not be ensured because the corresponding solution may lie in the infeasible region between b and c. Thus, only if we have enough samples near the boundary (i.e. line b), this method can find the true boundary and derive desirable solutions with guaranteed optimality and feasibility. Conversely, even if we only have a small number of samples near the boundary, the proposed regression-based model can utilize the safe distances of samples to exactly identify the specific position of the boundary. Thus, it can achieve better performance than the classification-based method in practice.

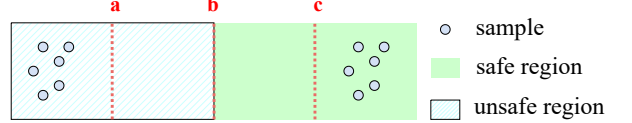


Fig. 3. An example case to illustrate why the classification-based method can not guarantee optimality and feasibility.

### C. Learning-based model for power loss calculation

As mentioned in Section II-A, the net active power at the substation, i.e.,  $G_t^g$  can be calculated based on Eq. (8). In Eq. (8), the term  $\mathbf{1}^\top \mathbf{p}_t$  is easy to obtain because  $\mathbf{p}_t$  is the controllable variable. However, the total power loss  $l_t$  is affected by the line current on each branch. Traditionally, these line currents are calculated based on the power flow model. Thus, if the topology is unavailable, the value of  $l_t$  is hard to obtain. To overcome this challenge, we train another regression MLP to predict the power loss without the topology. Then, the power loss can be expressed as

$$\mathbf{h}_t^{0,l} = \mathbf{x}_t, \quad \forall t \in \mathcal{T}, \quad (27)$$

$$\mathbf{z}_t^{k,l} = \mathbf{W}^{k,l} \mathbf{h}_t^{k-1,l} + \mathbf{b}^{k,l}, \quad \forall k \in \mathcal{K}^l, \forall t \in \mathcal{T}, \quad (28)$$

$$\mathbf{h}_t^{k,l} = \max(\mathbf{z}_t^{k,l}, 0), \quad \forall k \in \mathcal{K}^l, \forall t \in \mathcal{T}, \quad (29)$$

$$l_t = \mathbf{W}^{K+1,l} \mathbf{h}_t^{K,l} + \mathbf{b}^{K+1,l}, \quad \forall t \in \mathcal{T}. \quad (30)$$

After training, parameters  $\mathbf{W}^{k,l}$  and  $\mathbf{b}^{k,l}$  can be obtained. Then, power loss calculation can be replicated by the forward propagation of the trained MLP, i.e., Eqs. (27)-(30).

**Remark 1.** In essence, the proposed method trains three regression MLPs to approximate power flow constraints, i.e., Eqs. (7)-(11), in which only historical data (i.e. power injections, bus voltages and line currents) are required. Then, the voltage, current limitations and power loss calculation can be replicated by the forward propagation of the trained MLPs, i.e., Eqs. (23)-(26) and (27)-(30).

### D. Reformulation of the regression-based model

The forward propagation of the trained MLPs, i.e., constraints (23)-(26) and (27)-(30), build the mappings from power injections to the safe distances and power loss. As mentioned in Section III-A, the voltage and current limitations require nonnegative safe distances, i.e. Eq. (20). Then, based on Eqs. (20), (23)-(26) and (27)-(30), the voltage/current limitations and power loss calculation be replicated without the network topology. However, due to the inside maximum operator, constraints (25) and (29) are intractable and can not be directly handled by off-the-shelf solvers. Thus, a linearization technique is required to make these constraints tractable. Inspired by [27], we reformulate Eqs. (24)-(25) and (28)-(29) into tractable linear constraints based on the big-M method by introducing auxiliary variables  $r_t^{k,\{v,c,l\}}$  and

$\mu_t^{k,\{v,c,l\}}$ , as follows:

$$\begin{cases} \mathbf{h}_t^{k,\{v,c,l\}} - \mathbf{r}_t^{k,\{v,c,l\}} = \mathbf{W}^{k,\{v,c,l\}} \mathbf{h}_t^{k-1,\{v,c,l\}} + \mathbf{b}^{k,\{v,c,l\}}, \\ 0 \leq \mathbf{h}_t^{k,\{v,c,l\}} \leq M \cdot \mu_t^{k,\{v,c,l\}}, \\ 0 \leq \mathbf{r}_t^{k,\{v,c,l\}} \leq M \cdot (1 - \mu_t^{k,\{v,c,l\}}), \\ \mu_t^{k,\{v,c,l\}} \in \{0, 1\}^{N_k^{\{v,c,l\}}}, \end{cases} \quad \forall k \in \mathcal{K}^{\{v,c,l\}}, \forall t \in \mathcal{T}, \quad (31)$$

where  $M$  is a big enough constant. Then, the original problem **P1** can be reformulated into **P2**, which is defined as follows:

$$\begin{aligned} & \min_{q_t^e, \forall t \in \mathcal{T}} \sum_{t=1}^T (EC_t - R_t), \\ & \text{s.t.: Eqs. (2)-(10), (13)-(17),} \\ & \quad \{(20), (23), (26)-(27), (30)-(31)\}^{\{\wedge, -, \vee\}}. \end{aligned} \quad (\text{P2})$$

**Remark 2.** Neural networks are traditionally considered as “black box” models that are not convenient for optimization problems. In this section, we reformulate the proposed MLPs into “white box” linear constraints with binary variables. Then, the proposed TCL power scheduling problem **P1** can be reformulated as a mixed-integer linear program, **P2**. It then can be solved efficiently by off-the-shelf solvers. Moreover, the optimality of solutions can be also guaranteed.

**Remark 3.** We select MLPs instead of other state-of-art learning-based models, such as Convolutional Neural Networks [28], Recurrent Neural Networks [29], [30], and Generative Adversarial Networks [31], to replicate the power flow calculation. This is because we can easily convert MLPs into tractable mixed-integer linear forms, while the rest models are hard to reformulate. Thus, MLPs are more appropriate for the OPF-based power scheduling than other models.

#### E. Procedure of the proposed method

Our key idea is to replace the power flow equations with MLPs so that the power flow security constraints and power loss calculation can be considered without the exact topology. To better illustrate the key idea, we present the whole procedure of the proposed method in Fig. 4. This method is composed of the following four steps:

- 1) **Data prepare:** collect the historical data, including power injections, bus voltages, and line currents. Then, use this data to calculate the total power loss and safe distances based on Eqs. (8), (18), and (19).
- 2) **MLP training:** train three MLPs for predicting current, voltage safe distances, and power loss. Power injections of samples are treated as inputs (features) of all three MLPs. The current, voltage safe distances, and power loss of samples are regarded as the outputs (labels) of the three regression MLPs.
- 3) **MLP reformulation:** The trained MLPs can not be directly treated as constraints in the optimization due to the maximum operator in the ReLU activation function. Thus, we reformulate Eqs. (24)-(25) and (28)-(29) into linear constraints with binary variables, i.e. Eq. (31).

TABLE I  
PARAMETERS IN CASE STUDY

Parameters	Value	Parameters	Value
$C_i$	16.7 kWh/°C	$\theta$	24°C
$R_i$	0.3 °C/kW	$\bar{\theta}$	28°C
$COP_i$	3.6	$\bar{P}$	0.1MW
$\phi_i$	0.1	$\bar{Q}$	0.03MW
$\delta$	0.1		

Then, the whole optimization problem becomes a mixed-integer linear problem, which can be solved efficiently by off-the-shelf solvers with guaranteed optimality.

- 4) **Solving P2:** solve **P2** with the given heat loads and power demands. Output the optimal operation strategy for HVAC systems and PV plants.

It should be noted that if the topology of the distribution system is changed by reconfiguration, the trained MLPs might be inaccurate. However, in practice, there is usually only a few switches for topology reconfiguration so that the number of typical topology scenarios is very limited [32]. Since the reconfiguration is usually controlled by the system operators, the required switching state information is also known. As a result, it is trivial for the operators to collect historical operational data and train the MLPs for each different topology scenario, respectively. Hence, the proposed model can be readily extended to consider the scenarios with distribution system reconfiguration operations.

Compared with the published model-free methods introduced in Section I, the proposed learning-based method has several advantages. Firstly, the proposed model is a mixed-integer linear programming so that it can achieve guaranteed optimality based on the mature branch-and-bound algorithm. Moreover, it only needs the operational data and does not require the topology information. In addition, based on the safe distances, the feasible/infeasible boundaries can be well identified with no need for a large amount of data near the boundaries. Therefore, it can achieve better performance compared to the classification-based methods.

## IV. CASE STUDY

### A. Simulation set up

The case study is based on the IEEE 123-bus system with 14 installed PV plants, as shown in Fig. 5. The slack bus voltage, i.e.,  $V_1$ , is 2.40kV. The optimization time horizon is 24h and the time step  $\Delta t$  is 1h. The total heat load  $\mathbf{h}_t^h$ , total available PV generation  $G_t^{\max}$ , ambient temperature  $\theta_t^{\text{out}}$ , active base load  $p_t^e$  and reactive base load  $q_t$  are illustrated in Fig. 6. The unit prices for electricity purchasing/selling and upward/downward regulations as shown in Fig. 7, which are from [33], [34] and also adopted in [10]. Other parameters are summarized in Table I.

We conducted a comprehensive simulation based on Pandapower, a power system simulation toolbox in Python environment [35], to generate the historical data. In Pandapower, the power flow calculation is based on the full AC power flow model. The feasible region  $\mathcal{S}$  is constructed based on the voltage constraint (i.e. all bus voltages should stay in [0.9 p.u.,

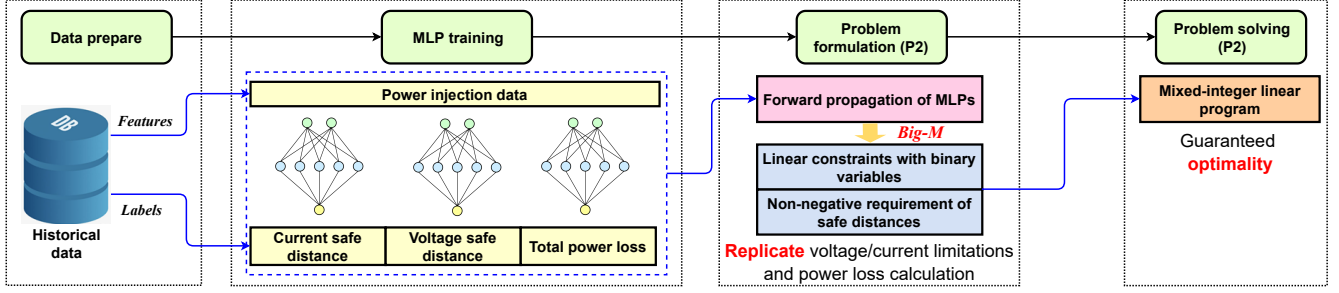


Fig. 4. Procedure of the proposed learning-based method.

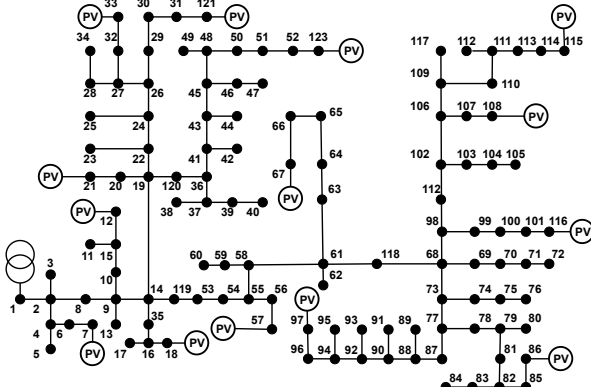


Fig. 5. Structure of the IEEE 123-bus test system.

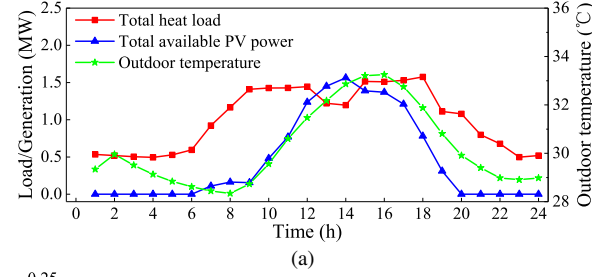


Fig. 6. (a) Total heat load, ambient temperature, available PV generation, and (b) total active/reactive based loads (except the demands of HVAC systems).

1.1 p.u.) and current constraint (i.e. all line currents should be less than 0.421 kA). We randomly generate bus injection vectors  $\mathbf{x}_t$  and give them to Pandapower to calculate the state variable  $s_t$ . Then, the safe distances of these generated samples (i.e.  $d_t^y$  and  $d_t^c$ ) and the corresponding power loss can be calculated according to Eqs. (18), (19), and (8). We gather  $(\mathbf{x}_t, d_t^y)$ ,  $(\mathbf{x}_t, d_t^c)$  and  $(\mathbf{x}_t, l_t)$  to construct the training set for the three regression MLPs, respectively. Finally, 20,000 samples are generated as the historical dataset for each MLP. We have also provided all the samples in [36].

All numerical experiments are implemented on an Intel(R) 8700 3.20GHz CPU with 16 GB memory. Our MLPs are constructed and trained by Pytorch (batch size and maximum epoch number are 256 and 500). To mitigate the overfitting of

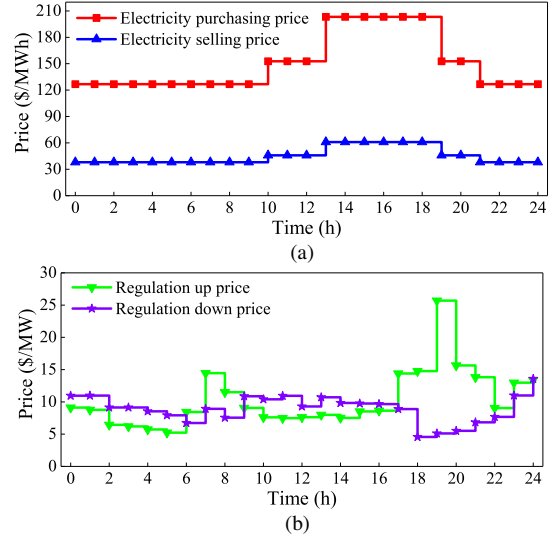


Fig. 7. Prices of (a) electricity purchasing/selling and (b) regulation up/down.

MLPs, we adopt the dropout technique proposed in reference [37] during MLP training. We employ CVXPY to build our optimization problem and GUROBI to solve it.

## B. Benchmarks

To demonstrate the feasibility and optimality of the proposed model, three benchmarks are introduced:

- 1) **B1:** Adopt the proposed model **P1** but ignoring the security operation constraint (11);
- 2) **B2:** Adopt the proposed model **P1** and utilize DistFlow model (relaxed as a second order cone) to describe constraint (11);
- 3) **B3:** Adopt the proposed model **P1** but utilize the binary classification MLP adopted in references [24], [25] to judge whether constraint (11) is satisfied or not.

Note that **B2** can be regarded as an ideal method with assumption that accurate topology is available. The learning-based method **B3** requires no topology information of the distribution network. In its dataset, the features keep the same as those in the proposed model, while the labels are determined by the following rule: if the state variable  $s_t$  of a sample satisfies Eq. (20), it is labeled as “safe”; otherwise, “unsafe”. In the optimization step, we restrict the output as “safe” for **B3** to ensure the safe operation. For each model, the power scheduling of TCLs in all the three scenarios (i.e. baseline scenario for  $G_t^{g,-}$ , upper bound scenario for  $G_t^{g,\wedge}$  and lower bound scenario for  $G_t^{g,\vee}$ ) are optimized simultaneously. Then,

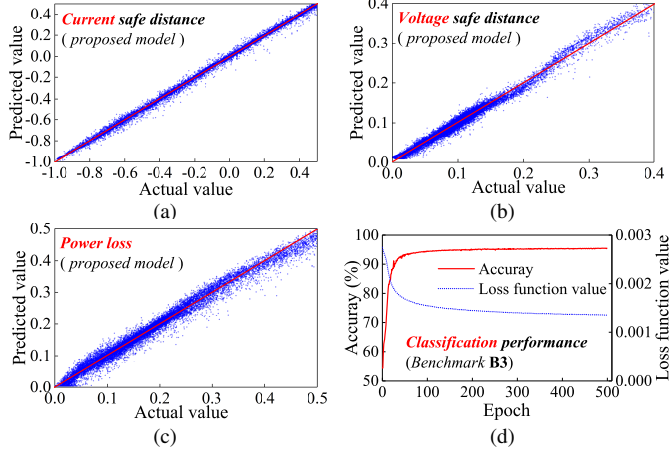


Fig. 8. Performances of the four trained MLPs for (a) predicting current safe distance in the **proposed model** (b) predicting voltage safe distance in the **proposed model**, (c) predicting power loss in the **proposed model**, and (d) classifying safe/unsafe operation state in **B3**.

all solutions are given to Pandapower again to obtain the actual total costs, voltage and currents for validation.

### C. Model feasibility, optimality, and time-efficiency

1) *Performance of trained MLPs:* Altogether four MLPs are trained in our simulation. The first three are regression MLPs and belong to the proposed model for the predictions of current, voltage, safe distances and power loss. The forth MLP belongs to **B3** and is used for the safe/unsafe classification. After careful hyper-parameter tuning, we set the hidden layer numbers of all MLPs as 1. The corresponding neuron numbers are set as 20 (for predicting current safe distance), 5 (for predicting voltge safe distance), 5 (for predicting power loss) and 100 (for classification in **B3**). Fig. 8 demonstrates the training results of the above four MLPs. In Figs. 8(a), (b), and (c), the horizontal and vertical axes are the actual and predicted safe distances. The red line represents the position where the prediction is equal to its actual value. Obviously, all samples are very close to the red line, which implies the high prediction accuracy of the three regression MLPs.

Although the accuracy of the classification MLP reaches to 95%, as shown in Fig. 8(c), this result still can not confirm that the safe/unsafe boundary is well described. Suppose there are 5% of the samples near the safe/unsafe boundary, then the classification accuracy can still reach to 95% even all boundary data is incorrectly classified. In other words, this high accuracy may be majorly contributed by the samples far away from the boundary. In that case, **B3** may derive low-quality solutions if it needs to make decisions that are close to the boundaries.

2) *Current and voltage:* In the upper bound scenario, the system tries to maximize its total net load at substation to enlarge the regulation capacity. Hence, the power flow in each branch grows until the security constraints (i.e. the voltage and current limitations) become active. In other words, this scenario is the riskiest and its optimal solution will lie on the safe/unsafe boundaries. Thus, we take the upper bound scenario as an example to illustrate the superiority of the proposed regression-based model. Fig. 9 presents the line current and bus voltage of different models in the upper bound scenario. Because that **B1** ignores the security constraint, its

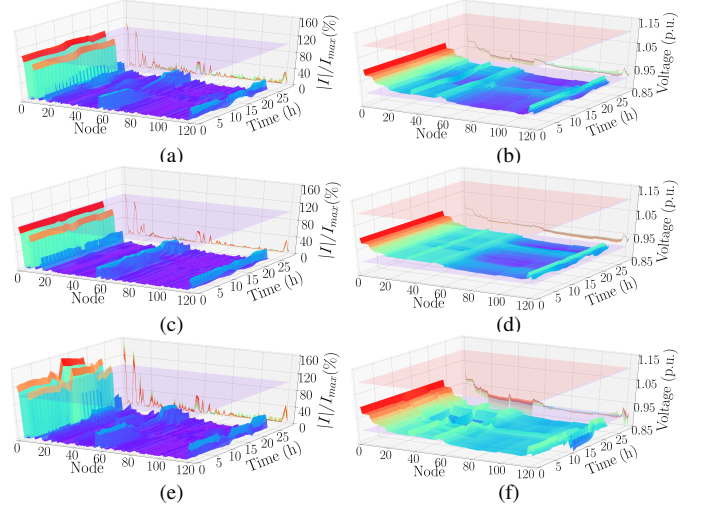


Fig. 9. (a) Line current of the proposed model, (b) bus voltage of the proposed model, (c) line current of **B2**, (d) bus voltage of **B2**, (e) line current of **B3**, and (f) bus voltage of **B3** in the upper bound scenario.

solution is infeasible for Pandapower. Thus, there is no result of **B1** in Fig. 9. The results of the proposed model are very similar to those of the power-flow-model-based model **B2**. Both the currents and voltages of the proposed model almost stay in the corresponding safe regions. Conversely, the line current of **B3** exceeds its upper boundary, and the bus voltage is also lower than 0.9 p.u. in many hours. As aforementioned, the proposed model can utilize the safe distance information to better identify the safe/unsafe boundaries. Thus, its solution can perform better feasibility compared to **B3**.

3) *Line current violations:* Fig. 10 illustrates the maximum line current violations of the upper and lower bound scenarios. Pandapower can not find a feasible result for **B1** due to the negligence of security constraint. **B3** replicates the power flow security constraints with a classification MLP. However, since the majority of the samples are far away from the feasible/infeasible boundaries, it fails to identify these boundaries accurately. Thus, its current violations are still quite significant, i.e., up to 56.03%. In contrast, the proposed method leverages the safe distances to pinpoint the boundaries, so the maximum current violation of the proposed method is only 8.78%, which is pretty close to the performance of the ideal method **B2**. These results confirm that the proposed model can derive better solutions with higher feasibility compared to **B3**.

Unlike the baseline and upper bound scenarios, the lower bound scenario tries to minimize the net load at substation or even sell surplus PV power to the upper-level grid (in that case, the total net load is negative). As shown in Fig. 10(b), the current violations only appear in the hours with high PV power when there is strong inverse power flow in the system. Similar to the upper bound scenario, the proposed model has similar performance with the ideal model **B2** and outperforms models **B1** and **B3**, significantly.

In the baseline scenario, the TCLs are coordinated to promote local PV generation consumption so that the power exchange between the main grid and distribution network is minimized. Hence, the power flow on each branch maintains at a low level, resulting in very small or even no violations in all of the four strategies, so we do not present the violation results of this scenario here.

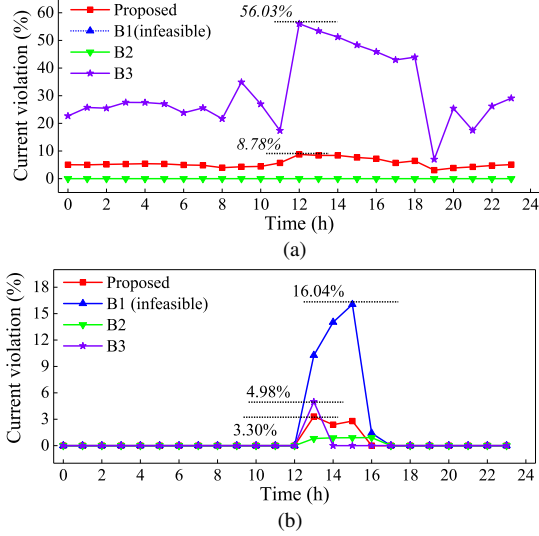


Fig. 10. Maximum line current violations in the (a) upper, and (b) lower bound scenarios.

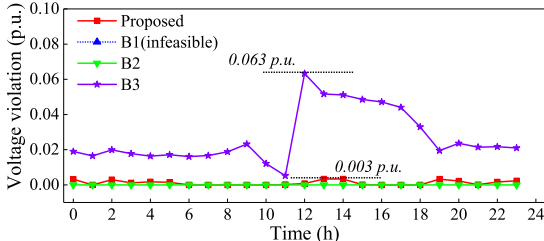


Fig. 11. Maximum bus voltage violations in the upper bound scenario.

4) *Bus voltage violations*: The bus voltage violations of the upper bound scenario are demonstrated in Fig. 11. The voltage violations in the lower bound and baseline scenarios are not shown here because they always maintain at a low level. In the upper bound scenario, **B1** derives the most dangerous solution, while **B2** achieves the lowest voltage violations but requires the network topology. The maximum voltage violation of **B3** is much larger than that of the proposed model (e.g. the maximum voltage violations of the proposed model and **B3** are 0.003p.u. and 0.063p.u., respectively). These results confirm that the proposed model can derive better solutions with higher feasibility compared to **B3**.

5) *Optimality of solutions*: The actual energy costs and regulation revenues are summarized in Table II. We treat the power flow model **B2** as our baseline. Obviously, the results of the proposed model are much closer to our baseline compared to the rest benchmarks. The total cost difference is around 2.20% between the proposed model and baseline, while this difference between **B3** and baseline reaches to 9.86%. Moreover, both **B1** and **B3** drastically overestimate the regulation revenues because they can not well describe the safe/unsafe boundaries. The gaps between the proposed and baseline models in the upward and downward revenues are 9.60% and 0.03%, while these gaps become 43.58% and 7.35% when **B2** is used. As for **B1**, these two gaps are infinite (the strategy for the upper bound scenario obtained by **B1** is infeasible for Pandapower) and 10.77%. These results indicate the great optimality of the proposed method.

6) *Time efficiency*: In the proposed learning-based method, three MLPs are reformulated into linear constraints with binary

TABLE II  
ENERGY COSTS AND REGULATION REVENUES

Model	Total Cost (\$)	Energy Cost (\$)	Upward revenue(\$)	Downward revenue(\$)
Proposed	559.62	780.53	171.30	49.63
<b>B1</b> <sup>1</sup>	—	786.93	—	55.00
<b>B2</b>	572.55	778.50	156.30	49.65
<b>B3</b>	516.10	793.82	224.42	53.30

<sup>1</sup> The corresponding solutions for the upper bound scenario is infeasible for Pandapower.

TABLE III  
TRAINING AND SOLVING TIMES OF THE PROPOSED METHOD

Time for MLP training (s)	Time for solving <b>P2</b> (s)
MLP1 <sup>1</sup>	MLP2 <sup>1</sup>
160.72	115.65
MLP3 <sup>1</sup>	98.69
	12.79

<sup>1</sup> MLP1, MLP2, MLP3 are regression MLPs used in the proposed method for predicting the current safe distance, voltage safe distance, and total power loss.

variables, which may lead to a large-scale mixed-integer linear problem and undesirable computational efficiency. To verify the computational performance of the proposed model, we summarize the solving time of different models in Table III. The proposed method achieves excellent computational efficiency, e.g., it only takes 12.79s for solving **P2**. This high computational efficiency may be contributed by hyper-parameter tuning. According to Eq. (31), the number of the introduced binary variables is the same as the MLP's neuron number. Thus, we have conducted a careful hyper-parameter tuning to minimize the neuron number while maintaining enough accuracy for predictions. The final neuron numbers are relatively small (i.e. 20, 5, and 5 for the MLPs for predicting the current, voltage safe distances, and power loss, respectively), so the computational burden of the proposed model can keep at an acceptable level.

In summary, the results in Figs. 8, 10, 11, and Table II demonstrate the excellent optimality, feasibility, and time-efficiency of the proposed learning-based OPF model, which confirms that the proposed model can accurately replicate the original power flow constraints with no need for the topology.

#### D. Effectiveness of the building thermal flexibility

In this subsection, we conduct an analysis study based on the results of the proposed model to demonstrate the effectiveness of utilizing building thermal flexibility.

1) *Net load profiles*: Fig. 12 illustrates the actual net load profile and its lower and upper bounds. In our simulation, the net active power  $G_t^g$  is always limited by the line current constraint between bus 1 and 2. Thus, the absolute value of the active net power in the upper bound scenario, i.e.,  $|G_t^{g,\wedge}|$ , almost keeps constant<sup>3</sup>. In the hours with low PV power (i.e.

<sup>3</sup>We observe that the value of  $|G_t^{g,\wedge}|$  is approximately equal to  $I_{12,\max} V_1$ . The objective of the upper bound scenario is to maximize  $G_t^{g,\wedge}$ . Considering that the total reactive power demand are much smaller than the total active demand in our case study, we have  $|s_{1,t}^\wedge| = \sqrt{(G_t^{g,\wedge})^2 + (q_{1,t}^\wedge)^2} = I_{12,t}^\wedge V_1 \approx |G_t^{g,\wedge}|$ , where  $|s_{1,t}^\wedge|$  is the magnitude of the apparent power injection on the slack bus. Besides, the line current limitation requires  $I_{12,t}^\wedge \leq I_{12,\max}$ . Based on this, we know that  $G_t^{g,\wedge}$  can take its maximum value at  $I_{12,t}^\wedge = I_{12,\max}$ . Then, we have  $|G_t^{g,\wedge}| \approx I_{12,\max} V_1$ .

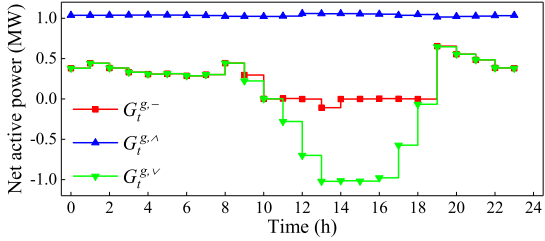


Fig. 12. Actual net load profile and its upper and lower bounds.

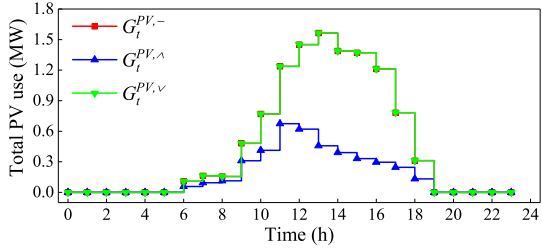


Fig. 13. Total PV generation in the baseline, lower and upper bound scenarios.

0:00am-11:00am and 18:00pm-24:00pm), the lower bound  $G_t^{g,V}$  are almost the same with the actual net load profile  $G_t^{g,-}$  because there is no extra PV power to sell. In the rest hours, a lot of PV power is sold to the upper-level grid in the lower bound scenario, while the extra PV power is converted as cooling power and stored in building thermal inertia in the baseline scenario. Thus, the lower bound profile is smaller than the baseline and becomes negative in these hours, which indicates that negative line currents appear in our simulation. Nevertheless, the lower bound  $G_t^{g,V}$  is still restricted by the line current limitation, so its magnitude is also close to  $I_{12,\max} V_1$ . These results confirm that the proposed method can work well with negative line currents in the system.

2) *Actual PV generation:* The actual PV generation is shown in Fig. 13. The actual PV generation keeps the same with the available PV power in both the baseline and lower bound scenarios. As aforementioned, the surplus PV is sold to the upper-level grid in the lower bound scenario, while it is locally consumed in the baseline scenario. In contrast, the upper bound scenario curtail part of the PV generation to maximize the net load. As a result, there is a distinct gap between the available and actual PV generation.

3) *Local storage of PV power:* Fig. 14 illustrates the total heat load, cooling supply and indoor temperature variation of the baseline scenario. The total heating load is the summation of indoor contributed heat loads and heat transfer from the outdoor environment (i.e.  $q_{i,t}^h + (\theta_t^{\text{out}} - \theta_{i,t}^{\text{in}})/R_i$ ). In the first few hours, the available PV power is small, so the cooling supply is identical to the heat load. From 11:00 am to 16:00 pm, the PV generation can fully cover the demands, and the extra PV is converted into cooling power and stored in building inertia locally for the later use. Thus, the cooling supply is obviously higher than the heating load and significant temperature drops occur in indoor environments. In the afternoon, the available PV power decreases gradually and can not cover the power consumption any more. Then, the stored cooling power is released to compensate the demands, so the indoor

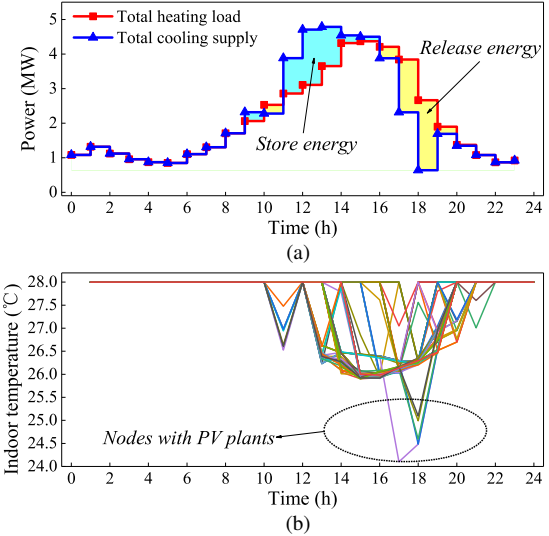


Fig. 14. Results of (a) total heating load and cooling supply, and (b) indoor temperatures of all buildings in the baseline scenario.

temperatures grow up gradually. As shown in Fig. 14(b), the temperature drops in the PV nodes (i.e. nodes with installed PV plants) are much faster and more significant than the non-PV nodes during 12:00 am to 16:00 pm, which shows storing and consuming PV generation locally is more economic.

## V. CONCLUSIONS

A learning-based OPF model is proposed to optimize TCL power schedules to improve operational flexibility for regulation service and minimize the energy cost minus regulation revenue. To involve the power flow security constraints, the proposed model trains two regression MLPs based on the historical operation data, which does not require the network topology information that is often unavailable. To guarantee the optimality of solutions, the trained MLPs are further reformulated into linear constraints with binary variables. As a result, the proposed model becomes a mixed-integer programming that can be effectively solved by off-the-shelf solvers. Simulation results demonstrate that the proposed method can achieve better feasibility performance with much less security constraint violations than published benchmark methods. The derivation between the total costs of the proposed model and an ideal power-flow-based model is less than 1%, which confirms the high optimality of our approach. The results also prove the effectiveness of utilizing building thermal inertia to promote local renewable generation integration.

Note the core of the proposed model is the learning-based OPF model, so it can be also applied to many other OPF-based application cases, such as optimal coordination of distribution networks and electric vehicles [38], economic dispatch of combined heat and power units [39], and optimal power dispatch of electricity-gas network [40].

Since the proposed model is based on historical data, it may not work well in cases without enough data. Thus, we envision our future work to extend the proposed method so that it can be applied to those cases with few historical data.

## REFERENCES

- [1] IEA, “Renewables 2020.” [OL]. <https://www.iea.org/reports/renewables-2020> Accessed November, 2020.
- [2] M. Islam, M. Nadarajah, and M. J. Hossain, “Short-term voltage stability enhancement in residential grid with high penetration of rooftop pv units,” *IEEE Trans. Sustain. Energy*, vol. 10, no. 4, pp. 2211–2222, 2019.
- [3] H. Zhao, B. Wang, Z. Pan, H. Sun, Q. Guo, and Y. Xue, “Aggregating additional flexibility from quick-start devices for multi-energy virtual power plants,” *IEEE Trans. Sustain. Energy*, vol. 12, no. 1, pp. 646–658, 2021.
- [4] R. Hemmati, H. Mehrjerdi, M. Shafie-khah, P. Siano, and J. P. S. Catalão, “Managing multitype capacity resources for frequency regulation in unit commitment integrated with large wind ramping,” *IEEE Trans. Sustain. Energy*, vol. 12, no. 1, pp. 705–714, 2021.
- [5] J. Li, F. Liu, Z. Li, C. Shao, and X. Liu, “Grid-side flexibility of power systems in integrating large-scale renewable generations: A critical review on concepts, formulations and solution approaches,” *Renew. Sust. Energ. Rev.*, vol. 93, pp. 272–284, 2018.
- [6] Y. Shi, B. Xu, D. Wang, and B. Zhang, “Using battery storage for peak shaving and frequency regulation: Joint optimization for superlinear gains,” *IEEE Trans. Power Syst.*, vol. 33, no. 3, pp. 2882–2894, 2018.
- [7] X. Zhang, G. Hug, J. Z. Kolter, and I. Harjunkoski, “Demand response of ancillary service from industrial loads coordinated with energy storage,” *IEEE Trans. Power Syst.*, vol. 33, no. 1, pp. 951–961, 2018.
- [8] A. Kathirgamanathan, M. De Rosa, E. Mangina, and D. P. Finn, “Data-driven predictive control for unlocking building energy flexibility: A review,” *Renew. Sust. Energ. Rev.*, vol. 135, p. 110120, 2020.
- [9] G. Chicco, S. Riaz, A. Mazza, and P. Mancarella, “Flexibility from distributed multienergy systems,” *Proc. IEEE*, vol. 108, no. 9, pp. 1496–1517, 2020.
- [10] H. Hao, D. Wu, J. Lian, and T. Yang, “Optimal coordination of building loads and energy storage for power grid and end user services,” *IEEE Trans. Smart Grid*, vol. 9, no. 5, pp. 4335–4345, 2018.
- [11] J. Wang, S. Huang, D. Wu, and N. Lu, “Operating a commercial building hvac load as a virtual battery through airflow control,” *IEEE Trans. Sustain. Energy*, vol. 12, no. 1, pp. 158–168, 2021.
- [12] F. A. Qureshi, I. Lympopoulos, A. A. Khatir, and C. N. Jones, “Economic advantages of office buildings providing ancillary services with intraday participation,” *IEEE Trans. Smart Grid*, vol. 9, no. 4, pp. 3443–3452, 2018.
- [13] X. Xu, Q. Lyu, M. Qadrدان, and J. Wu, “Quantification of flexibility of a district heating system for the power grid,” *IEEE Trans. Sustain. Energy*, vol. 11, no. 4, pp. 2617–2630, 2020.
- [14] Y. Jiang, C. Wan, A. Botterud, Y. Song, and S. Xia, “Exploiting flexibility of district heating networks in combined heat and power dispatch,” *IEEE Trans. Sustain. Energy*, vol. 11, no. 4, pp. 2174–2188, 2020.
- [15] M. Razmara, G. Bharati, D. Hanover, M. Shahbakhti, S. Paudyal, and R. D. Robinett III, “Building-to-grid predictive power flow control for demand response and demand flexibility programs,” *Appl. Energ.*, vol. 203, pp. 128–141, 2017.
- [16] X. Chen, E. Dall’Anese, C. Zhao, and N. Li, “Aggregate power flexibility in unbalanced distribution systems,” *IEEE Trans. Smart Grid*, vol. 11, no. 1, pp. 258–269, 2020.
- [17] Q. Shi, F. Li, G. Liu, D. Shi, Z. Yi, and Z. Wang, “Thermostatic load control for system frequency regulation considering daily demand profile and progressive recovery,” *IEEE Trans. Smart Grid*, vol. 10, no. 6, pp. 6259–6270, 2019.
- [18] H. Liu, H. Xie, H. Luo, J. Qi, H. H. Goh, and S. Rahman, “Optimal strategy for participation of commercial hvac systems in frequency regulation,” *IEEE Internet Things J.*, pp. 1–1, 2021.
- [19] L. Fabietti, T. T. Gorecki, F. A. Qureshi, A. Bitlislioğlu, I. Lympopoulos, and C. N. Jones, “Experimental implementation of frequency regulation services using commercial buildings,” *IEEE Trans. Smart Grid*, vol. 9, no. 3, pp. 1657–1666, 2018.
- [20] S. J. Pappu, N. Bhatt, R. Pasumarthy, and A. Rajeswaran, “Identifying topology of low voltage distribution networks based on smart meter data,” *IEEE Trans. Smart Grid*, vol. 9, no. 5, pp. 5113–5122, 2018.
- [21] B. J. Claessens, P. Vranx, and F. Ruelens, “Convolutional neural networks for automatic state-time feature extraction in reinforcement learning applied to residential load control,” *IEEE Trans. Smart Grid*, vol. 9, no. 4, pp. 3259–3269, 2018.
- [22] M. Al-Saffar and P. Musilek, “Reinforcement learning-based distributed bess management for mitigating overvoltage issues in systems with high pv penetration,” *IEEE Trans. Smart Grid*, vol. 11, no. 4, pp. 2980–2994, 2020.
- [23] X. Pan, T. Zhao, M. Chen, and S. Zhang, “Deepopf: A deep neural network approach for security-constrained dc optimal power flow,” *IEEE Trans. Power Syst.*, pp. 1–1, 2020.
- [24] A. Venzke, G. Qu, S. Low, and S. Chatzivasileiadis, “Learning optimal power flow: Worst-case guarantees for neural networks,” in *2020 IEEE International Conference on Communications, Control, and Computing Technologies for Smart Grids (SmartGridComm)*, pp. 1–7, 2020.
- [25] A. Venzke, D. T. Viola, and M. Jeanne, et al., “Neural networks for encoding dynamic security-constrained optimal power flow to mixed-integer linear programs,” *arXiv preprint arXiv:2003.07939*, 2020.
- [26] M. Baran and F. Wu, “Optimal sizing of capacitors placed on a radial distribution system,” *IEEE Trans. Power Deliv.*, vol. 4, no. 1, pp. 735–743, 1989.
- [27] M. Fischetti and J. Jo, “Deep neural networks and mixed integer linear optimization,” *Constraints*, vol. 23, no. 3, pp. 296–309, 2018.
- [28] S. Wang and H. Chen, “A novel deep learning method for the classification of power quality disturbances using deep convolutional neural network,” *Appl. Energy*, vol. 235, pp. 1126–1140, 2019.
- [29] Z. Shi, H. Liang, and V. Dinavahi, “Direct interval forecast of uncertain wind power based on recurrent neural networks,” *IEEE Trans. Sustain. Energy*, vol. 9, no. 3, pp. 1177–1187, 2018.
- [30] M. Khodayar and J. Wang, “Spatio-temporal graph deep neural network for short-term wind speed forecasting,” *IEEE Trans. Sustain. Energy*, vol. 10, no. 2, pp. 670–681, 2019.
- [31] Y. Chen, Y. Wang, D. Kirschen, and B. Zhang, “Model-free renewable scenario generation using generative adversarial networks,” *IEEE Trans. Power Syst.*, vol. 33, no. 3, pp. 3265–3275, 2018.
- [32] Z. Li, S. Jazebi, and F. de León, “Determination of the optimal switching frequency for distribution system reconfiguration,” *IEEE Trans. Power Deliv.*, vol. 32, no. 4, pp. 2060–2069, 2017.
- [33] “Open Access Same-Time Information System (OASIS), California Independent Syst. Oper., Folsom, CA, USA.” [Online]. <http://oasis.caiso.com>, accessed on Aug. 2016.
- [34] “Electric Rates, Pac. Gas Elect. Company, San Francisco, CA, USA.” [Online]. <http://www.pge.com/nots/rates/tariffs/electric.shtml>, accessed on Aug. 2016.
- [35] L. Thurner, A. Scheidler, F. Schafer, J. H. Menke, J. Dollichon, F. Meier, S. Meinecke, and M. Braun, “pandapower - an open source python tool for convenient modeling, analysis and optimization of electric power systems,” *IEEE Trans. Power Syst.*, 2018.
- [36] “Training sets.” [Online]. <https://github.com/lelouchsola/LearningTCLs>.
- [37] N. Srivastava, G. Hinton, A. Krizhevsky, I. Sutskever, and R. Salakhutdinov, “Dropout: a simple way to prevent neural networks from overfitting,” *J Mach Learn Res*, vol. 15, no. 1, pp. 1929–1958, 2014.
- [38] S. Huang, Q. Wu, J. Wang, and H. Zhao, “A sufficient condition on convex relaxation of ac optimal power flow in distribution networks,” *IEEE Trans. Power Syst.*, vol. 32, no. 2, pp. 1359–1368, 2017.
- [39] Y. Zhou, W. Hu, Y. Min, and Y. Dai, “Integrated power and heat dispatch considering available reserve of combined heat and power units,” *IEEE Trans. Sustain. Energy*, vol. 10, no. 3, pp. 1300–1310, 2019.
- [40] W. Dai, J. Yu, Z. Yang, H. Huang, W. Lin, and W. Li, “A static equivalent model of natural gas network for electricity–gas co-optimization,” *IEEE Trans. Sustain. Energy*, vol. 11, no. 3, pp. 1473–1482, 2020.